Hindawi
International Journal of Chemical Engineering
Volume 2022, Article ID 3112316, 9 pages
https://doi.org/10.1155/2022/3112316

Research Article

Rapid Determination of Mercury Ions in Environmental Water Based on an N-Rich Covalent Organic Framework Potential Sensor

Jinjin Tian and Yulin Zhu

Central South University of Forestry and Technology, Changsha, Hunan Province 410004, China

Correspondence should be addressed to Yulin Zhu; t20152270@csuft.edu.cn

Received 27 February 2022; Revised 4 June 2022; Accepted 16 June 2022; Published 9 July 2022

Academic Editor: Nicole Vorhauer-Huget

In this article, an N-rich covalent organic framework (COFTFPB-TZT) was successfully synthesized using 4,4′,4′-(1,3,5-triazine-2,4,6-triyl) trianiline (TZT), and 4-[3,5-bis (4-formyl-phenyl) phenyl] benzaldehyde (TFPB). The as-prepared COFTFPB-TZT possesses irregular cotton wool patches with a large specific surface area. A novel selective electrode based on $COF_{TFPB\text{-}TZT}$ was used for the determination of Mercury ions. The abundance of N atoms in $COF_{TFPB\text{-}TZT}$ provides more coordination sites for Hg^{2+} adsorption, resulting in a change in the surface membrane potential of the electrode to selectively recognize Hg^{2+}. Under optimal experimental conditions, the ion-selective electrode shows a good potential response to Hg^{2+}, with a linear range of 1.0×10^{-9}~1.0×10^{-4}, a Nernst response slope of 30.32 ± 0.2 mV/-PC at 25°C and a detection limit of 4.5 pM. At the same time, the mercury-ion electrode shows a fast response time of 10 s and good reproducibility and stability. The selectivity coefficients for Fe^{2+}, Zn^{2+}, As^{3+}, Cr^{6+}, Cu^{2+}, Cr^{3+}, Al^{3+}, Pb^{2+}, NH_4^+, Ag^+, Ba^{2+}, Mg^{2+}, Na^+, and K^+ are found to be small, indicating no interference in the detection system. The proposed method can be successfully applied to the determination of Hg^{2+} in 3 typical environmental water samples, with a recovery rate of 98.6–101.8%. In comparison with the spectrophotometric method utilizing dithizone, the proposed method is simple and fast and holds great potential application prospects in environmental water quality monitoring and other fields.

1. Introduction

Heavy metal pollution poses a great threat to human health and causes serious environmental problems. Mercury (Hg) is a highly toxic heavy metal element widely distributed in air, water, and soil [1]. Trace amounts of Hg^{2+} can produce strong toxicity and accumulate in the environment and organisms and can be transferred to the human body through the food chain, directly damaging the human brain, nervous system, kidney, and endocrine system [2, 3]. Therefore, the determination of Mercury ions is necessary in environmental monitoring and clinical analysis, and it is of great significance to improve the quality of human life and protect the Earth's environment. At present, mature methods for mercury-ion detection are as follows: spectrophotometry [4], inductively coupled plasma–mass spectrometry (ICP–MS) [5], atomic absorption/emission spectrometry (AAS/AES) [6], atomic fluorescence spectrometry (AFS) [7], high-performance liquid chromatography (HPLC) [8], inductively coupled plasma atomic emission spectrometry (ICP–AES) [9], and fluorescence probe detection [10]. Although these methods show excellent detection performance, most of them require expensive precision instruments, complex sample preparation processes, and skilled operators and cannot be conveniently used online or outdoors. Therefore, it is very important to find a simple, rapid, and inexpensive method for the determination of mercury-ion content.

The ion-selective electrode (ISE) method, as a rapid analytical tool, has been widely developed in the fields of the environment, medicine, and agriculture due to its advantages of fast speed, simple preparation, low cost, and high sensitivity [11]. In the process of preparing ion-carrier membranes with different selective electrodes, many organic, and inorganic complexes can be used as selective carriers of Mercury ions, such as crown ether [12], amide [13], glycidyl diamine [14], metalloporphyrin [15], Schiff

base [16], calixarene derivatives [17, 18], and alkylamine Mercury salt complexes [19]. Therefore, there is an urgent need to prepare Mercury ion-selective electrodes with good selectivity and a low detection limit. A large number of studies have proven that compounds containing N, O, and S atoms can form coordination compounds with heavy metal ions [20]. Mercury (II) shows a strong affinity with ligands containing sulphur atoms, such as sulfhydryl compounds [21], sulphur-containing heterocyclic rings [22], and thiourea derivatives [23], and its interaction relationship has been further verified by density functional theory calculations [24]. Many compounds containing sulphur atoms have been successfully used as active carriers for Mercury ion-selective electrodes [25]. Li et al. [26] prepared a simple and rapid Mercury ion selective electrode based on a 1-undecanethiol (1-UDT) PVC film electrode for the selective determination of Hg^{2+} ions, with a Nernst-response range and a detection limit of 4.5 nM. Fang et al. [27] reported a portable Hg^{2+} nanosensor using the CuS nanozyme functions as a Hg^{2+} recognition unit, which exhibits high sensitivity with a minimum detectable Hg^{2+} concentration of 50 ppt. Diamantis [28] et al. reported a microporous 8-connected Zr^{4+} metal-organic framework (MOF) based on a terephthalate ligand decorated with a chelating 2-picolylamine side group (dMOR-2), which shows a highly efficient fluorescence sensing and sorption of Mercury ions (Hg^{2+}), and the limits of detection were determined to be below 2 ppb for Hg^{2+}.

The covalent organic framework (COF) is a porous conjugated polymer that shows a large surface area, adjustable pore order, and easy functionalization [29–31]. In this study, a COF with an irregular cotton wool patch structure was synthesized from 4,4′,4′-(1,3,5-triazine-2,4,6-triyl) trianiline (TZT), and 4-[3,5-bis (4-formyl-phenyl) phenyl] benzaldehyde (TFPB). The as-prepared COF has ordered holes and a large specific surface area, and more N atoms will be exposed on the inner wall of the holes and the specific surface area of COF, providing more adsorption sites for the binding of Hg^{2+}. SEM and TEM characterization also prove the existence of such a recognition effect. The experimental results show that the electrode has high sensitivity, selectivity, reproducibility, and stability. The electrode is used for the rapid determination of Mercury ions in 3 typical environmental water samples and the results are compared with the spectrophotometric method with dithizone. The as-prepared $COF_{TFPB\text{-}TZT}$ shows excellent selectivity for Hg^{2+}, holding important application value in environmental monitoring, biomedical and agricultural product safety detection, and other fields.

2. Experimental Section

2.1. Reagents and Instruments. 4,4′,4′-(1,3,5-triazine-2,4,6-triyl) trianiline (TZT) and 4-[3,5-bis (4-formyl-phenyl) phenyl] benzaldehyde (TFPB) were obtained from Jilin Chinese Academy of Sciences Technology Co., Ltd. (Beijing, China). o-Dichlorobenzene (o-DCB), butyl alcohol (n-BuOH), dichloromethane (DCM), tetrahydrofuran (THF), N, N-dimethylformamide (DMF), acetic acid (AcOH), and Mercury chloride (Hg_2Cl) were purchased from Aladdin Biochemical Technology Co. Ltd. (Shanghai, China). Potassium ferricyanide (K_3 [Fe $(CN)_6$]), potassium ferrocyanide (K_4 [Fe $(CN)_6$]), sodium chloride (NaCl), disodium hydrogen phosphate ($Na_2HPO_4{\cdot}7H_2O$), sodium dihydrogen phosphate ($NaH_2PO_4{\cdot}7H_2O$), sodium sulphate (Na_2SO_4), chlorine (HCl), sulfuric acid (H_2SO_4, 98%), and hydrogen peroxide (H_2O_2, 30%) were purchased from Sinopharm Chemical Reagents Co. Ltd. (Shanghai, China). All chemicals used in the experiment were of analytical grade. Ultrapure water with a specific resistance larger than 18.3 $M\Omega{\cdot}cm^{-1}$ was used throughout the experiments.

The pH values were measured with a REXPHSJ-4A pH Meter (INESA Instrument Co. Ltd., China). All electrochemical measurements were performed using a CHI-760B workstation (Shanghai Chenhua Instruments Co., China). The potential values were detected with an Ollie Dragon Model 868 pH/mV meter (Thermo Orion, USA). Scanning electron microscopy (SEM) images were obtained using a Nova Nano230 (Thermo Fisher Scientific Co. Ltd., USA). Transmission electron microscopy (TEM) images were obtained using an FEI (Tecnai G2 F20 TMP, USA). The X-ray powder diffraction (XRD) spectrum was measured using a D/max-2500 diffractometer with a Cu Kα radiation source ($\lambda = 1.54056$ Å), Rigaku Co., Ltd., Tokyo), and a gas adsorption instrument (Micromeritics ASAP 2460 Sorptometer, MAC Instruments Co., Ltd., USA) was used to characterize the samples.

2.2. Synthesis of $COF_{TFPB\text{-}TZT}$ Material. First, 0.1 mol of TFPB and 0.1 mol of TZT were dissolved in 3 mL of dichloromethane (DCM)/n-butanol mixed solvent (1 : 1), followed by ultrasound treatment for 30 s. Next, 0.2 mL of 6.0 M acetic acid (AcOH) was added and poured into a Teflon-lined autoclave. Next, the reactor was heated at 120°C for 3 days. The precipitate obtained was repeatedly washed with dimethylformamide until the upper liquid became colourless. Meanwhile, the product was further purified by soaking in THF for 6 hours.

2.3. Electrode Preparation of $COF_{TFPB\text{-}TZT}$. A "piranha" solution was prepared by mixing 98% H_2SO_4 and 30% H_2O_2 at a volume ratio of 3 : 1 before being poured onto the surface of a gold plate electrode (GPE) for 1 min. The GPE was cleaned with ultrapure water and ethanol and dried with nitrogen for later use. Ethanol was ultrasonically dispersed with 1.5 mg $COF_{TFPB\text{-}TZT}$, and then the gold surface was immersed in 1.5 g/L $COF_{TFPB\text{-}TZT}$ ethanol solution and self-assembled at 4°C for 24 h. Finally, the $COF_{TFPB\text{-}TZT}$-modified electrode was washed with ethanol and ultrapure water, dried, and stored for later use.

3. Results and Discussion

3.1. Synthesis and Characterization of $COF_{TFPB\text{-}TZT}$. The morphology and structure of as-prepared $COF_{TFPB\text{-}TZT}$ before and after reacting with Mercury ions (Hg^{2+}) in solution was further characterized by transmission electron

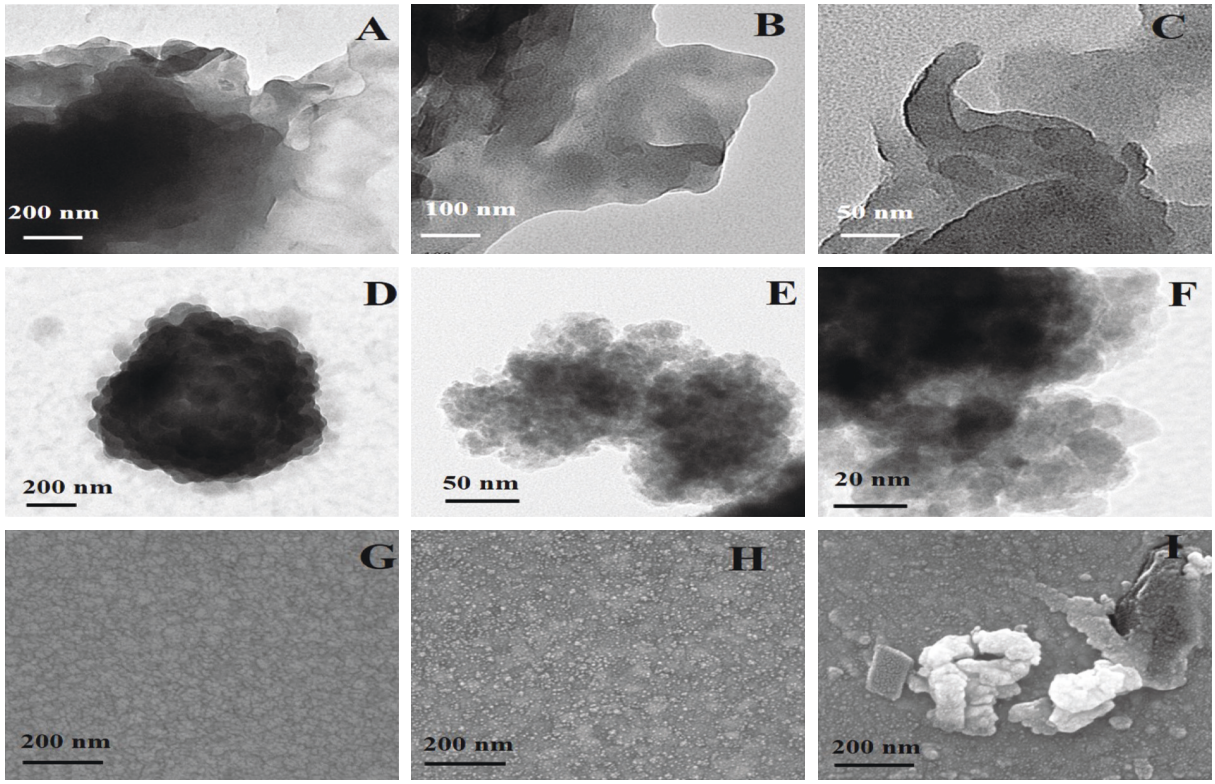

Figure 1: TEM images of $COF_{TFPB\text{-}TZT}$ (a–c) and $COF_{TFPB\text{-}TZT}/Hg^{2+}$ (d–f) at different magnifications. SEM images of bare GPE (g), GPE/$COF_{TFPB\text{-}TZT}$ (h), and GPE/$COF_{TFPB\text{-}TZT}/Hg^{2+}$ (i).

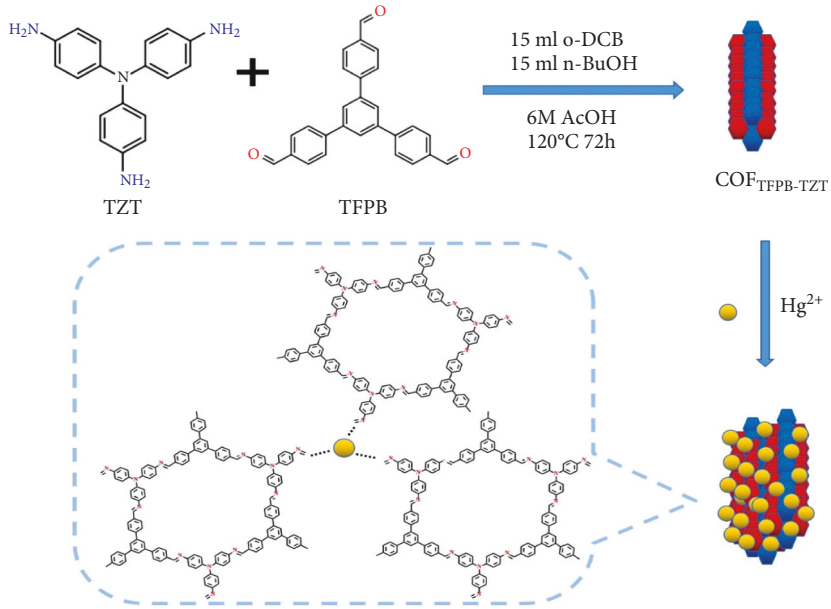

Scheme 1: Schematic illustration of the response process of the electrode.

microscopy (TEM). As shown in Figure 1, $COF_{TFPB\text{-}TZT}$ exhibits irregular cotton wool patches (Figures 1(a) ~1(c)). Upon the incorporation of Hg^{2+}, an amount of target Hg^{2+} is adsorbed onto the surface of irregular cotton wool patches via chemical chelation (Figures 1(d)–1(f)), and the irregular cotton wool patches are regathered into stacked layers of nano cotton. The change in the morphology of $COF_{TFPB\text{-}TZT}$ before and after the addition of Hg^{2+} is ascribed to the interaction between $COF_{TFPB\text{-}TZT}$ and Hg^{2+} via the chelation of chemical bonds. In addition, the surface morphology characteristics of the GPE/$COF_{TFPB\text{-}TZT}$ electrode before and after reacting with Mercury ions were tested by SEM, as shown in Figure 1(g) ~1(i). The naked gold plate electrode surface is observed to be very smooth (Figure 1(g)), and after

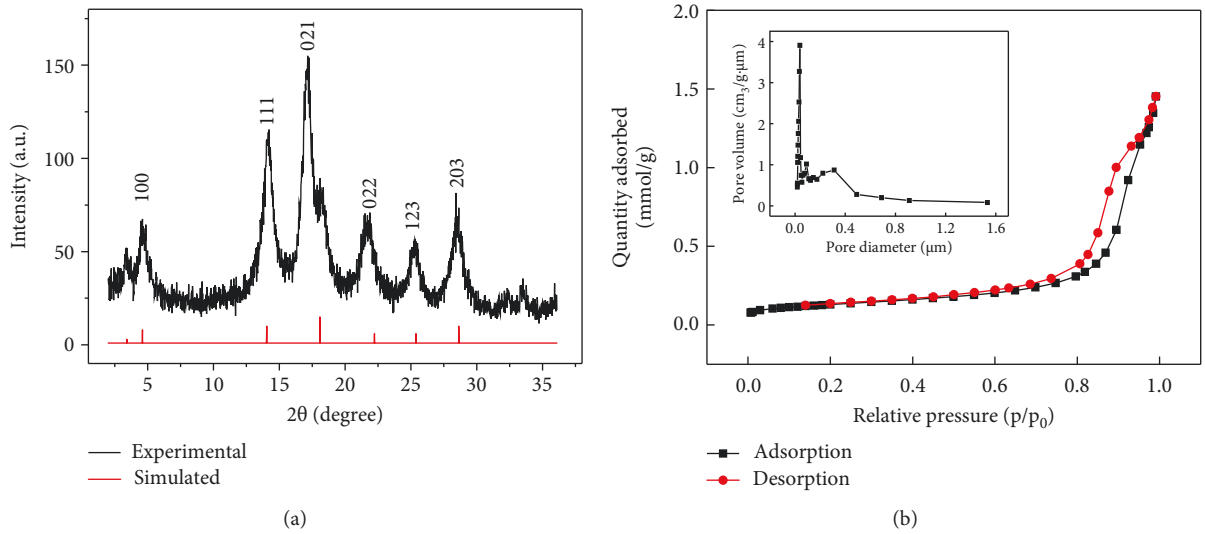

FIGURE 2: (a) Experimental (black curve) and simulated (red curve) XRD patterns for the as-prepared $COF_{TFPB\text{-}TZT}$. (b) N_2 adsorption-desorption isotherm (BET) for the as-prepared $COF_{TFPB\text{-}TZT}$. The insert shows the pore distribution of $COF_{TFPB\text{-}TZT}$.

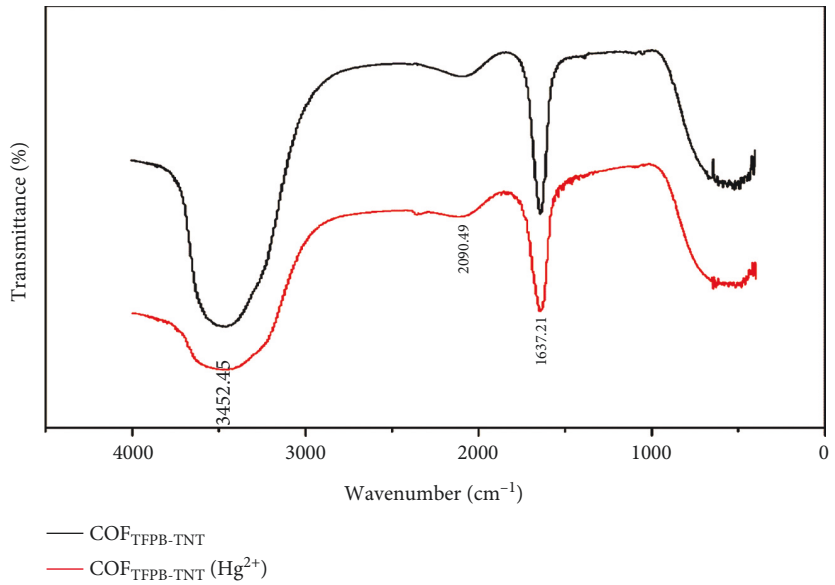

FIGURE 3: FT-IR spectra for the as-prepared $COF_{TFPB\text{-}TZT}$ (black curve) and $COF_{TFPB\text{-}TZT}/Hg^{2+}$ (red curve).

the self-assembly of $COF_{TFPB\text{-}TZT}$, the surface coverage becomes rough (Figure 1(h)). After testing in mercury-ion solution, the surface of the as-prepared $COF_{TFPB\text{-}TZT}$ changes significantly, and the electrode appears as larger agglomerates (Figure 1(i)). As shown in Scheme 1, the change in the structure can be ascribed to Mercury ions and amino functional groups of $COF_{TFPB\text{-}TZT}$ in the formation of strong coordination bonds, resulting in the complexes gathering strongly and changing the shape of the surface. Thus, different electron microscope images are presented.

The crystalline structure of $COF_{TFPB\text{-}TZT}$ was evidenced by X-ray diffraction (XRD) (Figure 2(a)), and the corresponding characteristic diffraction peaks for $COF_{TFPB\text{-}TZT}$ for the (100), (111), (021), (022), (023) and (203) planes are observed, which is in agreement with the simulated spectrum. In addition, adsorption-desorption isotherms (BET) were obtained to evaluate the specific surface area and pore size of the as-prepared $COF_{TFPB\text{-}TZT}$. The specific surface area of $COF_{TFPB\text{-}TZT}$ is deduced to be 80.9 $m^2 \cdot g^{-1}$, and the pore size of $COF_{TFPB\text{-}TZT}$ is 0.35 nm (Figure 2(b)), providing more active sites for Hg^{2+} ions. The XRD and BET results confirm that the as-prepared $COF_{TFPB\text{-}TZT}$ possesses a highly crystalline structure and ordered holes with a large specific surface area, providing more adsorption sites for the binding of Hg^{2+}. The N-atom rich composition of $COF_{TFPB\text{-}TZT}$ is responsible for the formation of $COF_{TFPB\text{-}TZT}/Hg^{2+}$, as evidenced by the FT-IR spectrum. As shown in Figure 3, the characteristic peak at 2390.49 cm^{-1} further proves the coordination relationship between the N element and Hg^{2+}. These results confirm that an N-rich covalent organic

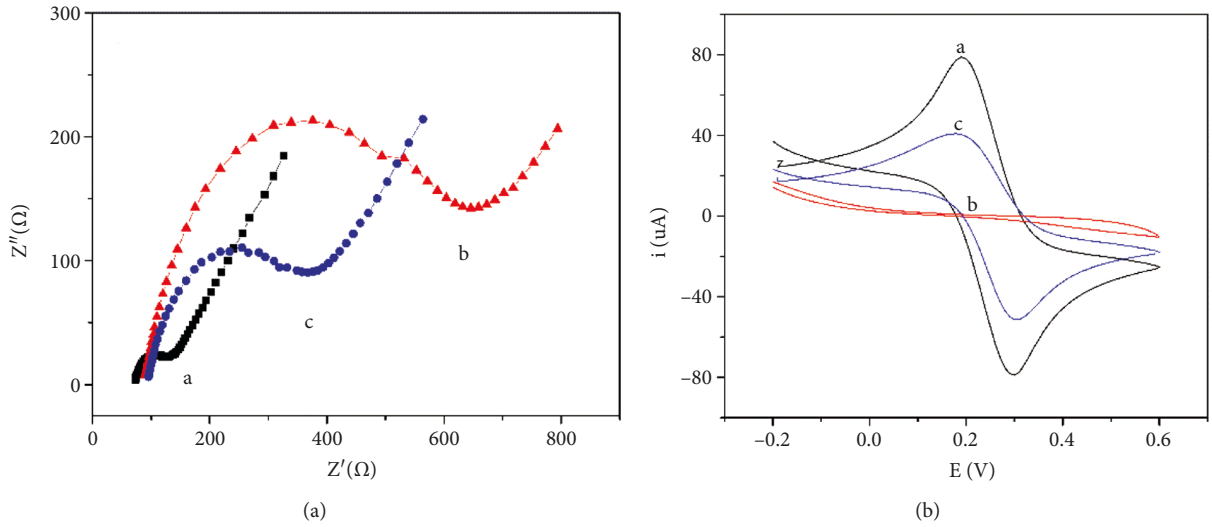

Figure 4: Electrochemical characteristic curves measured with impedance spectroscopy (a) and cyclic voltammetry (b) for bare GPE (A), GPE/COFTFPB-TZT (B), and GPE/$COF_{TFPB\text{-}TZT}$/Hg^{2+} (C) in a media solution containing 2.0 mmol/L $K_3Fe(CN)_6$ and 0.2 mol/L Na_2SO_4.

framework ($COF_{TFPB\text{-}TZT}$) can be successfully synthesized with 4,4′,4′-(1,3,5-triazine-2,4,6-triyl) trianiline (TZT), and 4-[3,5-bis (4-formyl-phenyl)phenyl]benzaldehyde (TFPB) reagent through the dehydration condensation reaction of amine aldehydes.

3.2. Electrochemical Characterization of $COF_{TFPB\text{-}TZT}$. To verify the interaction between the carrier and Mercury ion, the electrochemical behaviour of the different modified electrodes above was investigated by electrochemical impedance spectroscopy (EIS) and cyclic voltammetry (CV). As shown in Figure 4(a), curve a represents the bare gold plate electrode, and the impedance value is very small, indicating that the pretreated bare gold plate electrode has a strong ability to transfer electrons. Curve *b* represents the $COF_{TFPB\text{-}TZT}$-modified gold plate electrode. The semicircle appears in the high frequency part, and the impedance value increases significantly, indicating that $COF_{TFPB\text{-}TZT}$ forms a nonconductive monomolecular self-assembled film on the gold surface through the sulfhydryl group at one end, which hinders the electron conduction of $[Fe(CN)6]^{3-/4-}$ on the electrode surface. After combining Hg^{2+} (1.0×10^{-4} mol/L), the impedance value of the electrode decreases correspondingly (curve c), which is due to the strong coordination between the N element group and Hg^{2+} at the other end of $COF_{TFPB\text{-}TZT}$, which adsorbs positively charged Mercury ions and enhances the electronic conductivity, resulting in an electrochemical conduction current and reduced interfacial impedance. The variation trend for the impedance can also be verified by the corresponding cyclic voltammetry (Figure 4(b)). A pair of obviously reversible redox peaks in curve a is obtained, suggesting fast electron transfer at the bare gold plate electrode surface. Upon modification with $COF_{TFPB\text{-}TZT}$, the sharply decreased peak current in curve *b* indicates that the $COF_{TFPB\text{-}TZT}$ materials can hamper electron transfer to the electrode surface. When the $COF_{TFPB\text{-}TZT}$-modified electrode is treated with Hg^{2+} (curve c), the peak currents are slightly enhanced, which can be ascribed to the coordination of Mercury (II). The CV results are consistent with the above EIS results, indicating that this method is feasible for the identification and detection of Mercury ions.

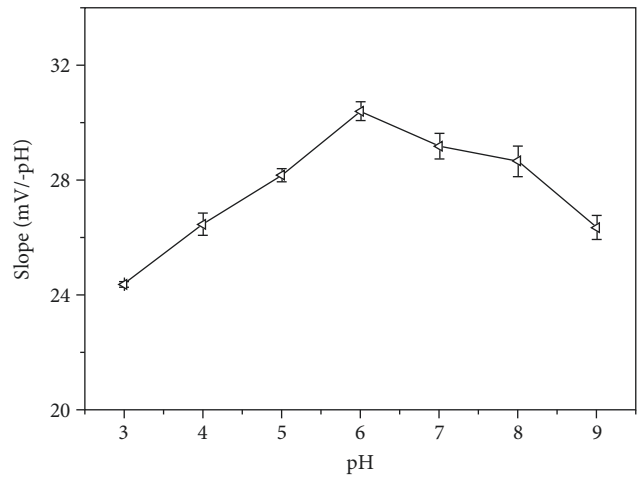

Figure 5: Effect of pH on the sensitivity of the GPE/$COF_{TFPB\text{-}TZT}$ electrode.

3.3. Optimal pH Selection. In the experiment, the relationship between the electrode potential and the concentration of the measured ionic solution at pH 3.0, 4.0, 5.0, 6.0, 7.0, 8.0, and 9.0 is discussed. The response slope was calculated and the relationship between the slope and pH was determined, as shown in Figure 3. As shown in Figure 5, the electrode presents a Nernst response to Hg^{2+} under acidic conditions (pH = 3.0~6.0). The electrode response slope shows the highest value at pH = 6.0, with a slope value of 30.32 ± 0.2 mV/-PC at 25°C, which is close to the theoretical value of the Nernst response slope of 29.58 mV/-PC [29–31]. The electrode slope at pH 3.0 and 4.0 is

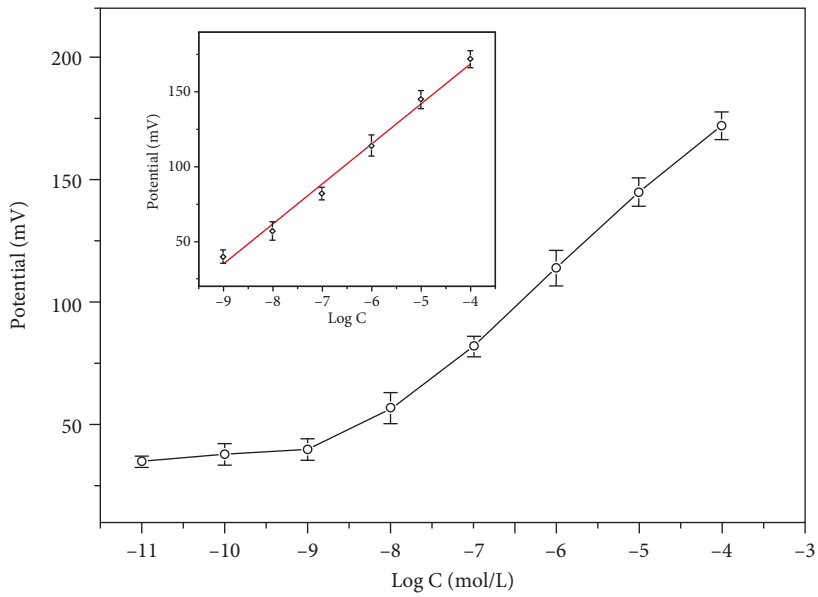

Figure 6: Potential response curve for the GPE/$COF_{TFPB\text{-}TZT}$ electrode to Hg^{2+} in Tris-HCl buffer (pH = 6.0). The concentrations of Hg^{2+} are 1.0×10^{-9}~1.0×10^{-4} mol/L. The inset shows the linear portions of the calibration curve. The error bars are absolute errors deduced from at least three replicate measurements, and the RSDs for all the concentrations are in the range of 3.3~11%.

Table 1: Comparison of various nanomaterials based on sensors for Hg^{2+} detection.

No.	Modified electrode	Linear range (μM)	LOD (nM)	Ref.
1	GCE/GA-UiO-66-NH_2	0.001–2.2	0.9	[32]
2	GCE/L-Cys-Cu_2O	0.33–3.3	0.02	[33]
3	GCE/NTOU4-nano-PANI	0.05–27.5	0.035	[34]
4	GCE/$ZnFe_2O_4$	10–100	80	[35]
5	GCE/ZIF-67/EG	-	1.28	[36]
6	GCE/Cu-MOFs	0.01–0.1	0.0048	[37]
7	GPE/$COF_{TFPB\text{-}TZT}$	0.001–100	0.0045	This work

Note: GCE: glassy carbon electrode; GA: graphene aerogel; NTOU4-nano: zinc phosphite framework nanoparticle; PANI: conductive polyaniline; ZIF-67: cobased zeolitic imidazolate framework; EG: expanded graphite; Cu-MOFs: metal-organic frameworks.

slightly smaller, which can be regarded as the nearly equal near-Nernst response slope. However, the slope of the response gradually decreases as the pH exceeds 6.0, which can be ascribed to the adverse reaction in the solution: $Hg^{2+} + OH^- \longrightarrow Hg(OH)^+$. The decrease in slope originates from a small amount of Hg^{2+} being converted to $Hg(OH)^+$ for the formation of insoluble salts, leading to a reduction in the concentration of Mercury ions at pH > 6.0. In addition, an insoluble Mercury salt produced in an alkaline solution (pH > 7.0) is likely to adhere to the electrode surface, leading to electrode damage. Therefore, the optimal pH value was selected to be 6.0.

3.4. Electrode Response Performance. The test response performance of GPE/$COF_{TFPB\text{-}TZT}$ to Hg^{2+} was investigated in the experiment. Figure 6 shows the potential response curve of the electrode combined with different concentrations of Hg^{2+} in Tris-HCl buffer solution (pH = 6.0). As shown in Figure 6, the electrode potential gradually increases with increasing Hg^{2+} concentration, indicating that the bonding of Hg^{2+} on the modified electrode surface increases. In addition, the electrode shows a good linear response to Hg^{2+} ions in the concentration range of 1.0×10^{-9}~1.0×10^{-4} mol/L in Tris-HCl buffer solution at pH = 6.0. The linear equation fitted by the least square method is $\delta E = 276.08 + 26.82 \log C$ ($R^2 = 0.9873$). The lower limit of detection can be deduced to be 4.5×10^{-12} mol/L according to the plotting method. Comparing the GPE/$COF_{TFPB\text{-}TZT}$ with other modified electrodes reported using different nanomaterials [32–37], as shown in Table 1, it can be seen that the $COF_{TFPB\text{-}TZT}$-modified biosensor in this work has better properties with a wider linear range and higher sensitivity.

3.5. Determination of Response Time, Stability, and Reproducibility. The response time and stability of the GPE/$COF_{TFPB\text{-}TZT}$-modified gold plate electrode for Hg^{2+} detection were investigated (Figure 7). The change in the dynamic potential curve after the addition of different concentrations of Hg^{2+} ions to Tris-HCl buffer solution was determined, namely, continuous measurements were carried out from low concentration to high concentration in the range of 1.0×10^{-9}~1.0×10^{-4} mol/L and the change in the potential value over time was recorded. The reaction time for the electrode to reach equilibrium in the whole concentration range is very short, which is calculated as 95% of the

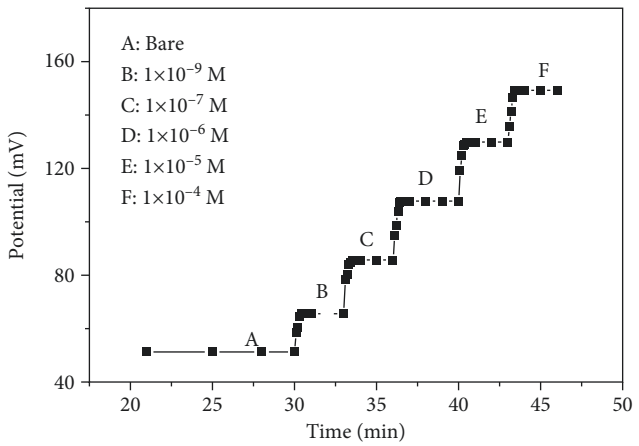

Figure 7: Dynamic response of the GPE/$COF_{TFPB\text{-}TZT}$ electrode to various concentrations of Hg^{2+} in Tris-HCl buffer (pH = 6.0).

maximum potential response, i.e., 20 s, indicating that the electrode has a fast response speed to Mercury ions. Then, the potential gradually tends to be stable with increasing time, indicating that the response performance of the electrode is stable. At the same time, the electrode was continuously monitored on a 1.0×10^{-7} mol/L Hg^{2+} sample for 25 min with a potential drift of +1.0 mV. The standard deviation for the potential data obtained is ± 2.22 mV, and the relative standard deviation is 1.72% ($n = 10$), indicating that the potential sensor has good stability. After the electrode was tested on Hg^{2+} samples for 15 days, the response slope of the electrode was changed to 20.5 mV/-PC, which decreased by 30.8%, indicating that the potential sensor can be used for at least half a month and has a long service life.

The potential response reproducibility of the GPE/$COF_{TFPB\text{-}TZT}$ electrode combined with different concentrations of Hg^{2+} samples was also investigated (Table 2); that is, the potential values of the 1.0×10^{-7} mol/L and 1.0×10^{-4} mol/L Hg^{2+} samples were measured back and forth 10 times. The relative standard deviations are 0.54% and 0.45%, respectively. The relative standard deviation is small, indicating that the electrode has good reproducibility.

3.6. Selectivity of the Electrode. In this experiment, the ion selectivity coefficient of the electrode was measured by the fixed interference ion concentration method (Figure 8), and the selectivity coefficient was calculated by using the Nicolskii–Eisenman formula [18].

$$K^{pot}_{Hg^{2+},M^{n+}} = \frac{a_{Hg^{2+}}}{a_{M^{n+}}}, \quad (1)$$

where $K^{pot}_{Hg^{2+},M^{n+}}$ represents the selectivity coefficient of Mercury ions, $a_{Hg^{2+}}$ represents mercury-ion activity, and $a_{M^{n+}}$ represents the activity of interfering ions. In the actual calculation, the ionic strength coefficient is ignored, and the activity is approximately replaced by the concentration. The selectivity coefficients for different metal ions (such as Fe^{2+}, Zn^{2+}, As^{3+}, Cr^{6+}, Cu^{2+}, Cr^{3+}, Al^{3+}, Pb^{2+}, NH_4^+, Ag^+, Ba^{2+}, Mg^{2+}, Na^+, and K^+) were investigated. The results show that the selectivity coefficients for these metal ions and oxidizing ions are relatively small, which does not interfere with the determination of Hg^{2+} by the electrode, indicating that the electrode shows good selectivity.

Table 2: Reproducibility of the GPE/$COF_{TFPB\text{-}TZT}$ electrode.

No.	Potential (mV)	
	1.0×10^{-6} mol/L	1.0×10^{-4} mol/L
1	97.0	140.0
2	96.3	139.3
3	97.0	140.0
4	95.6	140.0
5	96.3	139.2
6	96.2	138.5
7	97.1	139.2
8	97.0	139.3
9	96.3	140.0
10	97.0	140.7
AV	96.6	139.6
RSD	0.53%	0.45%

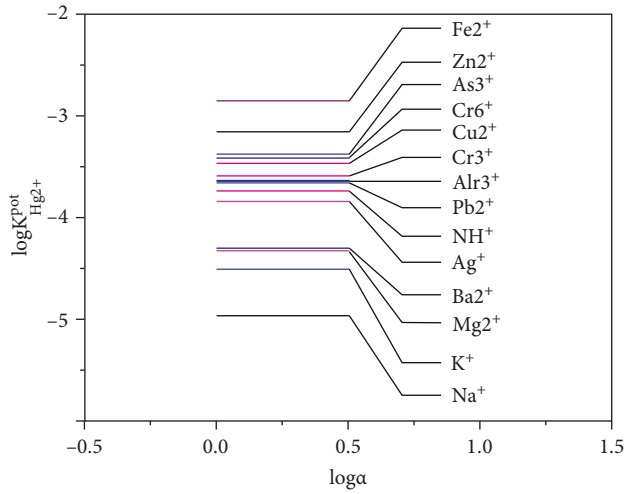

Figure 8: Selectivity coefficient of GPE/$COF_{TFPB\text{-}TZT}$ to Hg^{2+}.

3.7. Determination and Analytical Application of the Recovery Rate. To verify the practical applicability of the GPE/$COF_{TFPB\text{-}TZT}$ self-assembled gold plate electrode, the fabricated electrodes were used to detect Hg^{2+} in 3 typical water samples (river water, DI water, and polluted water) and compared with the spectrophotometric method with dithizone. As shown in Table 3, the concentration of Hg^{2+} measured by the GPE/$COF_{TFPB\text{-}TZT}$ self-assembled gold plate is consistent with that obtained by the spectrophotometric method with dithizone. Moreover, the recovery rates were found to vary in the range from 98.6% to 101.8%. According to the principle of the F test and T test in error analysis, the F value and T value for 6 samples were calculated, respectively, and the F value was determined to be 1.14, 2.14, 1.00, 2.86, 1.15, and 2.12, and the T value was determined to be 1.04, 1.06, 0.64, 0.30, 0.96, and 0.56, respectively. The above-given results indicate that the GPE/$COF_{TFPB\text{-}TZT}$ self-assembled gold plate electrode can be used

Table 3: Recovery of the proposed GPE/$COF_{TFPB\text{-}TZT}$ electrode for the determination of Mercury ions in real water samples compared with the spectrophotometric method utilizing dithizone.

Sample	Spiked	Spectrophotometric method with dithizone		GPE/DTT electrode		Recovery (%)
		(μmol/L)	SD	(μmol/L)	SD	
River water	0.500	0.502	±0.016	0.407	±0.015	101.8
River water	0.600	0.610	±0.013	0.491	±0.019	98.6
DI water	0.700	0.694	±0.014	0.604	±0.014	100.7
DI water	0.800	0.794	±0.013	0.797	±0.022	99.6
Pollution water	1.100	1.110	±0.015	1.106	±0.014	100.5
Pollution water	1.600	1.598	±0.011	1.596	±0.016	99.9

to determine Mercury ions in actual water samples. The spectrophotometric method with dithizone is a standard method for the detection of metal ions but requires a complex pretreatment process and involves organic reagents. In comparison with the spectrophotometric method utilizing dithizone, the proposed method is simple, easy to operate, fast, and holds great promise for environmental monitoring, biological medicine, and agricultural product safety testing.

4. Conclusion

A novel N-rich $COF_{TFPB\text{-}TZT}$ is prepared with the dehydration condensation reaction of amine aldehydes. A Hg^{2+-}selective electrode based on GPE/$COF_{TFPB\text{-}TZT}$ is developed based on a self-assembly method. In particular, $COF_{TFPB\text{-}TZT}$ contains many N elements, which provide abundant coordination sites for Hg^{2+}. The experimental results show that the GPE/$COF_{TFPB\text{-}TZT}$ electrode shows excellent performance with a wide linear response range of 1.0×10^{-9} ~1.0×10^{-4} mol/L and a short response time of 10 s, and the detection limit is determined to be 4.5 pM. In Tris-HCl buffer solution with pH = 6.0, the electrode potential electrode shows a good potential response to Hg^{2+} that meets the Nernst response. In comparison with the spectrophotometric method utilizing dithizone, the proposed method is simple and fast and holds great potential application prospects in environmental detection and biomedicine.

Data Availability

The data used to support the study are included in the paper.

Consent

Written informed consent for publication was obtained from all authors.

Conflicts of Interest

The authors declare that there are no conflicts of interest.

Acknowledgments

This work was financially supported by the following funds: Scientific Research Project of the Education Department of Hunan Province (Grant no. 18C0288)/Youth Scientific Research Fund Project of Central South University of Forestry and Technology (Grant no. 2016QY010)/Hunan Provincial Natural Science Foundation of China (Grant no. 2020JJ4950).

References

[1] K. Hua, X. L. Xu, Z. P. Luo, D. Fang, R. Bao, and J. H. Yi, "Effective removal of mercury ions in aqueous solutions: a review," *Current Nanoscience*, vol. 16, no. 3, pp. 363–375, 2020.

[2] X. Geng, W. Zhao, Q. Zhou, Y. Duan, T. Huang, and X. Liu, "Effect of a mechanochemical process on the stability of mercury in simulated fly ash. part 1. ball milling," *Industrial & Engineering Chemistry Research*, vol. 60, no. 41, pp. 14737–14746, 2021.

[3] Y. Yang, J. Liu, and Z. Wang, "Reaction mechanisms and chemical kinetics of mercury transformation during coal combustion," *Progress in Energy and Combustion Science*, vol. 79, Article ID 100844, 2020.

[4] H. J. Chun, S. Kim, Y. D. Han et al., "Water-soluble mercury ion sensing based on the thymine-Hg^{2+}-thymine base pair using retroreflective janus particle as an optical signaling probe," *Biosensors and Bioelectronics*, vol. 104, pp. 138–144, 2018.

[5] A. Srivastava, S. E. Long, J. E. Norris, C. E. Bryan, J. Carney, and J. T. Hodges, "Comparison of primary laser spectroscopy and mass spectrometry methods for measuring mass concentration of gaseous elemental mercury," *Analytical Chemistry*, vol. 93, no. 2, pp. 1050–1058, 2021.

[6] Z. Gajdosechova, E. Pagliano, A. Zborowski, and Z. Mester, "Headspace in-tube microextraction and GC-ICP-MS determination of mercury species in petroleum hydrocarbons," *Energy and Fuels*, vol. 32, no. 10, pp. 10493–10501, 2018.

[7] A. Kiss and A. Gaspar, "Fabrication of a microfluidic flame atomic emission spectrometer: a flame-on-a-chip," *Analytical Chemistry*, vol. 90, no. 10, pp. 5995–6000, 2018.

[8] I. H. Hsu, T. C. Hsu, and Y. C. Sun, "Gold-nanoparticle-based graphite furnace atomic absorption spectrometry amplification and magnetic separation method for sensitive detection of mercuric ions," *Biosensors and Bioelectronics*, vol. 26, no. 11, pp. 4605–4609, 2011.

[9] N. Bansal, J. Vaughan, A. Boullemant, and T. Leong, "Determination of total mercury in bauxite and bauxite residue by flow injection cold vapour atomic absorption spectrometry," *Microchemical Journal*, vol. 113, pp. 36–41, 2014.

[10] D. Sánchez-Rodas, W. T. Corns, B. Chen, and P. B. Stockwell, "Atomic fluorescence spectrometry: a suitable detection technique in speciation studies for arsenic, selenium,

antimony and mercury," *Journal of Analytical Atomic Spectrometry*, vol. 25, no. 7, p. 933, 2010.

[11] K. Huang, K. L. Xu, X. D. Hou, Y. Jia, C. Zheng, and L. Yang, "UV-induced atomization of gaseous mercury hydrides for atomic fluorescence spectrometric detection of inorganic and organic mercury after high performance liquid chromatographic separation," *Journal of Analytical Atomic Spectrometry*, vol. 28, no. 4, p. 510, 2013.

[12] A. Manna, A. K. Maharana, G. Rambabu, S. Nayak, S. Basu, and S. Das, "Dithia-crown-ether integrated self-exfoliated polymeric covalent organic nanosheets for selective sensing and removal of mercury," *ACS Applied. Polymer Materials*, vol. 3, no. 11, pp. 5527–5535, 2021.

[13] R. Bhatt, S. Kushwaha, S. Bojja, and P. Padmaja, "Chitosan-thiobarbituric acid: a superadsorbent for mercury," *ACS Omega*, vol. 3, no. 10, pp. 13183–13194, 2018.

[14] Z. H. Wu, J. H. Lin, and W. L. Tseng, "Oligonucleotide-functionalized silver nanoparticle extraction and laser-induced fluorescence for ultrasensitive detection of mercury (II) ion," *Biosensors and Bioelectronics*, vol. 34, no. 1, pp. 185–190, 2012.

[15] D. Peng, L. Zhang, R. P. Liang, and J. D. Qiu, "Rapid detection of mercury ions based on nitrogen-doped graphene quantum dots accelerating formation of manganese porphyrin," *ACS Sensors*, vol. 3, no. 5, pp. 1040–1047, 2018.

[16] A. Kumar, M. Dubey, R. Pandey et al., "A Schiff base and its copper (II) complex as a highly selective chemodosimeter for mercury (II) involving preferential hydrolysis of aldimine over an ester group," *Inorganic Chemistry*, vol. 53, no. 10, pp. 4944–4955, 2014.

[17] M. Park, K. I. Hong, S. M. Jin, E. Lee, W. D. Jang, and S. Y. Ju, "Helical assembly of flavin mononucleotides on carbon nanotubes as multimodal near-IR Hg (II)-selective probes," *ACS Applied Materials and Interfaces*, vol. 11, no. 8, pp. 8400–8411, 2019.

[18] M. Retout, P. Blond, I. Jabin, and G. Bruylants, "Ultrastable PEGylated calixarene-coated gold nanoparticles with a tunable bioconjugation density for biosensing applications," *Bioconjugate Chemistry*, vol. 32, no. 2, pp. 290–300, 2021.

[19] S. Tyagi, H. Agarwal, and S. Ikram, "Potentiometric polymeric membrane electrodes for mercury detection using calixarene ionophores," *Water Science and Technology*, vol. 61, no. 3, pp. 693–704, 2010.

[20] F. Vakili, A. Rashidi, L. Taghavi, and N. Mansouri, "Single-step synthesis of N, S co-doped waste-derived nanoporous carbon sorbent for mercury vapor removal," *Environmental Science and Pollution Research*, vol. 28, no. 14, pp. 17265–17274, 2021.

[21] Q. Wang, S. Zhu, C. Xi, B. Jiang, and F. Zhang, "Adsorption and removal of mercury (II) by a crosslinked hyperbranched polymer modified via sulfhydryl," *ACS Omega*, vol. 7, no. 14, pp. 12231–12241, 2022.

[22] L. Xing, M. Li, T. Qi et al., "Construction of confined bifunctional 2D material for efficient sulfur resource recovery and Hg^{2+} adsorption in desulfurization," *Environmental Science and Technology*, vol. 56, no. 7, pp. 4531–4541, 2022.

[23] R. Barzaga, L. Lestón-Sánchez, F. Aguilar-Galindo, O. Estévez-Hernández, and S. Díaz-Tendero, "Synergy effects in heavy metal ion chelation with aryl- and aroyl-substituted thiourea derivatives," *Inorganic Chemistry*, vol. 60, no. 16, pp. 11984–12000, 2021.

[24] Y. Ling, J. Wu, B. Li, and D. Liu, "Insights into the mechanism of elemental mercury adsorption on graphitic carbon nitride: a density functional theory study," *Energy and Fuels*, vol. 35, no. 11, pp. 9322–9331, 2021.

[25] L. K. Lin, J. T. Tsai, S. Díaz-Amaya et al., "Antidelaminating, thermally stable, and cost-effective flexible kapton platforms for nitrate sensors, mercury aptasensors, protein sensors, and p-type organic thin-film transistors," *ACS Applied Materials and Interfaces*, vol. 13, no. 9, pp. 11369–11384, 2021.

[26] X. Q. Li, H. Q. Liang, Z. Cao et al., "Simple and rapid mercury ion selective electrode based on 1-undecanethiol assembled Au substrate and its recognition mechanism," *Materials Science and Engineering: C*, vol. 72, pp. 26–33, 2017.

[27] Y. Fang, Y. Zhang, L. Cao et al., "Portable Hg^{2+} nanosensor with ppt level sensitivity using nanozyme as the recognition unit, enrichment carrier, and signal amplifier," *ACS Applied Materials and Interfaces*, vol. 12, pp. 1211761–1211768, 2020.

[28] S. A. Diamantis, A. D. Pournara, E. D. Koutsouroubi et al., "Detection and sorption of heavy metal ions in aqueous media by a fluorescent Zr (IV) metal-organic framework functionalized with 2-picolylamine receptor groups," *Inorganic Chemistry*, vol. 61, no. 20, pp. 7847–7858, 2022.

[29] Q. Sun, B. Aguila, J. Perman et al., "Postsynthetically modified covalent organic frameworks for efficient and effective mercury removal," *Journal of the American Chemical Society*, vol. 139, no. 7, pp. 2786–2793, 2017.

[30] X. Zhong, Z. Lu, W. Liang, and B. Hu, "The magnetic covalent organic framework as a platform for high-performance extraction of Cr (VI) and bisphenol a from aqueous solution," *Journal of Hazardous Materials*, vol. 393, Article ID 122353, 2020.

[31] Y. Jiang, C. Liu, and A. Huang, "EDTA-functionalized covalent organic framework for the removal of heavy-metal ions," *ACS Applied Materials and Interfaces*, vol. 11, no. 35, pp. 32186–32191, 2019.

[32] M. Lu, Y. Deng, Y. Luo et al., "Graphene aerogel-metal-organic framework-based electrochemical method for simultaneous detection of multiple heavy-metal ions," *Analytical Chemistry*, vol. 91, no. 1, pp. 888–895, 2019.

[33] X. Pang, H. Bai, H. Zhao et al., "Biothiol-functionalized cuprous oxide sensor for dual-mode sensitive Hg^{2+} detection," *ACS Applied Materials and Interfaces*, vol. 13, no. 39, pp. 46980–46989, 2021.

[34] Y. Li, J. F. Xie, C. C. Chang, C. M. Wang, and H. L. Tu, "Highly sensitive detection of mercury ions using zincophosphite framework nanoparticle–polyaniline composites," *ACS Applied Nano Materials*, vol. 3, no. 10, pp. 9724–9730, 2020.

[35] C. C. Fan, L. Chen, R. Jiang et al., "$ZnFe_2O_4$ nanoparticles for electrochemical determination of trace Hg (II), Pb (II), Cu (II), and glucose," *ACS Applied Nano Materials*, vol. 4, pp. 4026–4036, 2021.

[36] L. F. Ma, X. Y. Zhang, M. Ikram, M. Ullah, H. Wu, and K. Y. Shi, "Controllable synthesis of an intercalated ZIF-67/EG structure for the detection of ultratrace Cd^{2+}, Cu^{2+}, Hg^{2+} and Pb^{2+} ions," *Chemical Engineering Journal*, vol. 395, Article ID 125216, 2020.

[37] X. Zhang, M. Zhu, Y. Jiang et al., "Simple electrochemical sensing for mercury ions in dairy product using optimal Cu^{2+}-based metal-organic frameworks as signal reporting," *Journal of Hazardous Materials*, vol. 400, Article ID 123222, 2020.